Earthquake Geotechnical Engineering for Protection and Development of Environment and Constructions – Silvestri & Moraci (Eds)
© 2019 Associazione Geotecnica Italiana, Rome, Italy, ISBN 978-0-367-14328-2

Analysis of buried oil and gas pipelines crossing active faults: Revisiting pipe-ground interaction

G. Kouretzis
Priority Research Centre for Geotechnical Science and Engineering, Faculty of Engineering and Built Environment, The University of Newcastle, Australia

G. Bouckovalas
School of Civil Engineering, National Technical University of Athens, Greece

ABSTRACT: Despite recent developments in computer modelling, the analysis in practice of buried oil and gas steel pipelines crossing active faults usually relies on simplified numerical and analytical beam-on-nonlinear Winkler foundation models. This paper presents recent experimental measurements and numerical estimates of the developing soil reaction, as function of relative soil-pipe movement, used as input in Winkler analysis models. First, we discuss techniques developed to physically model relative soil-pipe movements, as well as imaging-based methods used to document mechanisms of pipe-backfill interaction. Next, we present advanced numerical methods for the analysis of complex pipe-backfill-trench geometries, used to quantify the resistance provided by native stiff soil/rock on pipes backfilled with sand. The presentation concludes with new insights on the mechanics of soil-pipe interaction and recommendations for its modelling in practice, focusing on scenarios not covered by existing guidelines, such as deeply buried pipes and pipes laid in trenches excavated in stiff soil/rock.

1 INTRODUCTION

It is common for pipeline networks in regions of high seismicity to cross the trace of active faults. In the event of rupture of such a fault, a step-like deformation will be imposed on the pipe. The magnitude of this deformation may be even of the order of meters, and usually will result to failure with the form of buckling or tensile rupture of even high-strength continuous welded steel pipes, unless special mitigation measures are implemented. A number of buried pipe failures due to fault rupture were observed during the Chi-Chi, Taiwan earthquake (Uzarski & Arnold 2001), the Kocaeli, Turkey earthquake (EERI 1991) but also the less well-known Tennant Creek, Australia earthquake, which resulted in severe damage of the 14-in Amadeus Basin-to-Darwin gas pipe (Figure 1). However, if designed properly, pipes can survive such extreme actions. Owing to its ingenious design, the Trans-Alaska 48-in oil pipeline survived the 2002 rupture of the Denali strike-slip fault, which gave the M=7.9 Denali fault earthquake, and resulted in 5.5m horizontal and 1m vertical movement of the ground surface at the vicinity of the pipe (Hall et al. 2003).

Today, analysis methods for buried pipes against differential ground movements are discussed in most guidelines for the design of buried steel pipes (e.g. ALA 2005, NEN3650 2003, PRCI 2009). Despite the fact that modern computational techniques allow for simulating the response of the three-dimensional pipe-soil system (e.g. Vazouras et al. 2010), the analysis tools described in guidelines and used in practice comprise either i) analytical methods based on the seminal work of Newmark and Hall (1975) (e.g. Karamitros et al. 2007, 2011, Trifonov & Cherniy 2010), or ii) beam-on-nonlinear Winkler foundation finite element models of the pipe and its surrounding soil. These methods allow capturing essential aspects of the problem, such geometric and material non-linearities, at a fraction of the cost of a three-dimensional finite element analysis. However, they also require as input the properties of non-linear

Figure 1. Failure of an API.5L X60 steel gas pipe during the 1999 Tennant Creek, Australia earthquake (source: Geosciences Australia).

Winkler springs representing soil reaction during relative soil-pipe movements along specific directions, instead of phenomenological soil and pipe parameters. Methods for estimating the properties of these springs have their origins to methods developed for estimating the pull-out capacity of plate anchors (e.g. Majer 1955, Dickin 1988). A number of experimental and numerical studies in the literature present methods for calculating the soil reaction to uplift (e.g. Trautman et al. 1985, White et al. 2008, Cheuk et al. 2008, Ansari et al. 2018a), lateral (e.g. Trautmann and O'Rourke 1985, Ansari et al. 2019), oblique (e.g. Jung et al. 2016) or vertical-downwards (Kouretzis et al. 2014, Limnaiou et al. 2019) relative movements.

One of the main assumptions underlying these methods for calculating spring properties is that longitudinal bending of the pipe and section deformation do not affect the reaction developing from soil. In other words, it is assumed that the pipe is rigid so that the problem of estimating the reaction on the pipe is reduced to a plane-strain one, which is much simpler to model physically and treat analytically or numerically. Large-scale experimental studies have shown that this simplification has a detrimental effect on the estimated soil reactions, particularly in the case of relatively flexible pipes (O'Rourke 2010, Palmer et al. 2006), thus it is usually ignored in practice.

Apart from that simplification, the field of application of current methods embraced in design guidelines is also limited to idealised scenarios, such as uniform backfill conditions around the pipe and "shallow" burial depths. In the following we will present some recent developments in experimental and numerical methods for estimating the properties of non-linear Winkler springs, when such idealised scenarios are not realistic. We will focus the discussion on the mechanisms leading to the development of soil reaction on the pipe, on numerical modelling techniques, and on results obtained for cases not covered in existing guidelines. Note that the results presented here are not applicable exclusively to the analysis of buried pipes crossing active faults, but can also be used for the analysis of pipes subjected to any ground deformation pattern, such as pipes crossings areas prone to subsidence (Kouretzis et al. 2015), liquefaction-induced lateral spreading, or active landslides. Furthermore, they can be used for estimating the capacity of pipes to resist thermal buckling, noting that while higher soil reaction will lead to increased pipe strains and therefore is detrimental in the case of fault rupture (or other imposed displacement problems), the opposite is true for thermal buckling problems.

The rest of the paper is organized as follows: First we present a recently developed experimental rig, designed and manufactured at the University of Newcastle, Australia, to physically model sand-pipe interaction in reduced scale, considering uniform (free field) backfill conditions. Details are provided on test conditions, including sand properties, followed by selected results that shed some light on the effect of sand density and problem geometry on the mechanisms of soil reaction development to pipe movements. Next, we discuss numerical methods for modelling soil-pipe interaction, focusing on the cases of pipes buried in narrow trenches excavated in stiff soil or rock, where the reaction to relative movements may be considerably higher compared to pipes in uniform sand. Finally we summarise recommendations for estimating Winkler spring properties for the analysis of pipes in practice, and for numerically modelling soil-pipe interaction.

2 PHYSICAL MODELLING OF UNIFORM SAND-PIPE INTERACTION

2.1 *Description of the testing rig*

The rig used to measure the reaction force on a rigid pipe during (oblique) pull-out, lateral drag but also pull-down tests in sand is depicted in Figure 2. Tests performed in this rig essentially mimic the displacement applied on a pipe during fault rupture, as the operator is able to control the orientation of the displacement (relatively to the pipe axis) through a set of adjustable pulleys. The design of the rig was inspired by other similar rigs described in the literature (e.g. Trautmann et al. 1985, Cheuk et al. 2008), but it allows modelling fault movements of arbitrary direction, unlike similar rigs which were designed to perform lateral drag or uplift tests only. The rig is fitted on a 2200mm x 2400mm steel frame, which accommodates a 1050mm (length) x 750mm (height) x 75mm (width) testing chamber, the components of the sand deposition system, the actuation system and the measuring instruments. The rig and the testing procedures are described in detail in Ansari et al. (2018a). Here we will only briefly explain the rationale behind the design of the rig, and key elements of the testing workflow.

The main goal of the design was to be able to measure with high accuracy the reaction developing on a rigid pipe as function of the magnitude and orientation of the prescribed displacement, for a very wide range of backfill sand densities, while achieving excellent sample uniformity. This renders the test results ideal for investigating mechanisms and benchmarking numerical simulations of soil-pipe interaction, keeping in mind that movement of a rigid object near the surface of a sand bed is challenging to model, as it involves large deformations (flow), material softening and frictional contact (Zhang et al. 2015). Therefore, we kept the dimensions of the chamber as small as possible and use pipes with diameters ranging from 37.5mm to 150mm (length-over-diameter ratio L/D=2 to 0.5, respectively). This facilitated the development of two custom sand deposition systems, that produce uniform sand beds with relative densities from D_r=19% up to D_r=92%. The excellent uniformity of the sand beds was verified via mini cone penetration tests, using a quality control system developed in parallel with the testing facility. In addition, the actuation system was designed to eliminate any fictitious kinematic constraints to pipe movements i.e. during a lateral displacement episode, as in the case of a pipe crossing a strike-slip fault, the pipe will move laterally relatively to its surrounding soil due to fault rupture, but also vertically due to the kinematics of pipe-soil interaction. As discussed in Zhang et al. (2015), the magnitude and the direction of this parasitic vertical component of pipe movement is a function of the shape and weight of the pipe, as well as the mechanical properties of sand, and will affect the shape of the developing failure surface and the lateral reaction on the pipe from sand. Finally, the glass windows of the chamber allow tracking of the evolution of the failure surface developing in sand as the pipe moves,

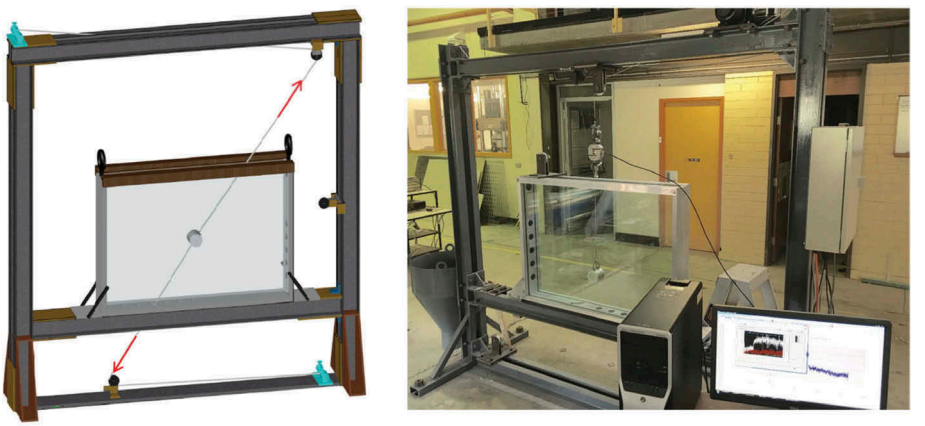

Figure 2. Schematic (left) and photo (right) of the physical modelling rig at the University of Newcastle laboratory.

using digital imaging equipment and a combination of the Particle Image Velocimetry (PIV) technique with close-range photogrammetry; specifically, the GeoPIV-RG software developed by White et al. (2013), and updated by Stanier et al. (2015).

2.2 *Test sand properties*

It is worth summarising here the properties of the silica sand used in the experiments. It is a uniform sand sourced from Stockton Beach, and is referred to in the following as STK sand. It has mean particle diameter D_{50}=0.36mm and maximum particle size D_{max}=0.62mm, while the rest of its physical properties are listed in Table 1. Two different, custom sand deposition methods were developed to prepare loose up to very dense sand beds. These methods are described in detail in Ansari et al. (2018a) and are not repeated here for brevity. The average sample unit weight and relative density achieved in the tests are listed in Table 2, noting that sand beds with unit weight deviating more that 0.25kN/m^3 from the values listed in Table 2 are disregarded, and the deposition is repeated. As mentioned earlier, the excellent uniformity of the sand beds was verified via a custom CPT profiling method, using a miniature cone with diameter 14mm fitting with a 222N mini load cell (Ansari et al. 2018a).

The shear strength and dilatancy potential of STK sand were determined using direct shear tests, using a custom setup capable of performing tests at normal stresses as low as σ_n=1.25kPa (Ansari et al. 2018a), as well as isotropically consolidated drained and undrained triaxial compression tests. In addition, its compressibility was characterised via incremental loading oedometer tests, performed with a custom cell fitted with bender elements to measure concurrently the shear wave propagation velocity. Results of these tests are summarised in Figure 3, which presents the variation of the peak plane strain friction angle φ_{ps}, the peak dilation angle ψ, and the coefficient of volume compressibility $1/m_v$ with normal stress. The plane strain friction angle φ_{ps} results from the friction angle obtained from direct shear tests φ_{ds} if we consider co-axiallity of stresses and incremental strains (Lings & Dietz 2004), using the expression derived by Davis (1968):

$$\tan \varphi_{ds} = \frac{\cos \psi \cdot \sin \varphi_{ps}}{1 - \sin \psi \cdot \sin \varphi_{ps}} \tag{1}$$

In addition to the above, the critical state friction angle of STK sand was determined to be φ_{cs}=32° from co-evaluation of the triaxial compression test results and measurements of the angle of repose.

It is worth mentioning here that O'Rourke (2010) used multiple linear regression analysis of physical modelling test results to derive an expression for an equivalent Young's modulus (Figure 3), appropriate for numerical modelling of soil-pipe interaction problems when the elastoplastic Mohr-Coulomb model is used to describe the behaviour of sand. In Figure 3 we

Table 1. Physical properties of STK sand.

D_{10} (mm)	D_{30} (mm)	D_{60} (mm)	C_u	C_c	e_{min}	γ_{min} (kN/m^3)	e_{max}	γ_{max} (kN/m^3)
0.18	0.27	0.38	2.11	1.06	0.51	14.5	0.79	17.2

Note: The maximum γ_{max} and minimum γ_{min} unit weight were measured according to the Australian Standard 1289 5.5.1.

Table 2 . Summary of test sand bed densities and associated deposition method.

Density	Average sand bed unit weight (kN/m^3)	Relative density D_r (%)	Deposition method
Loose	14.9	19	Pouring
Medium	16	58	Pouring
Loose	17	92	Raining

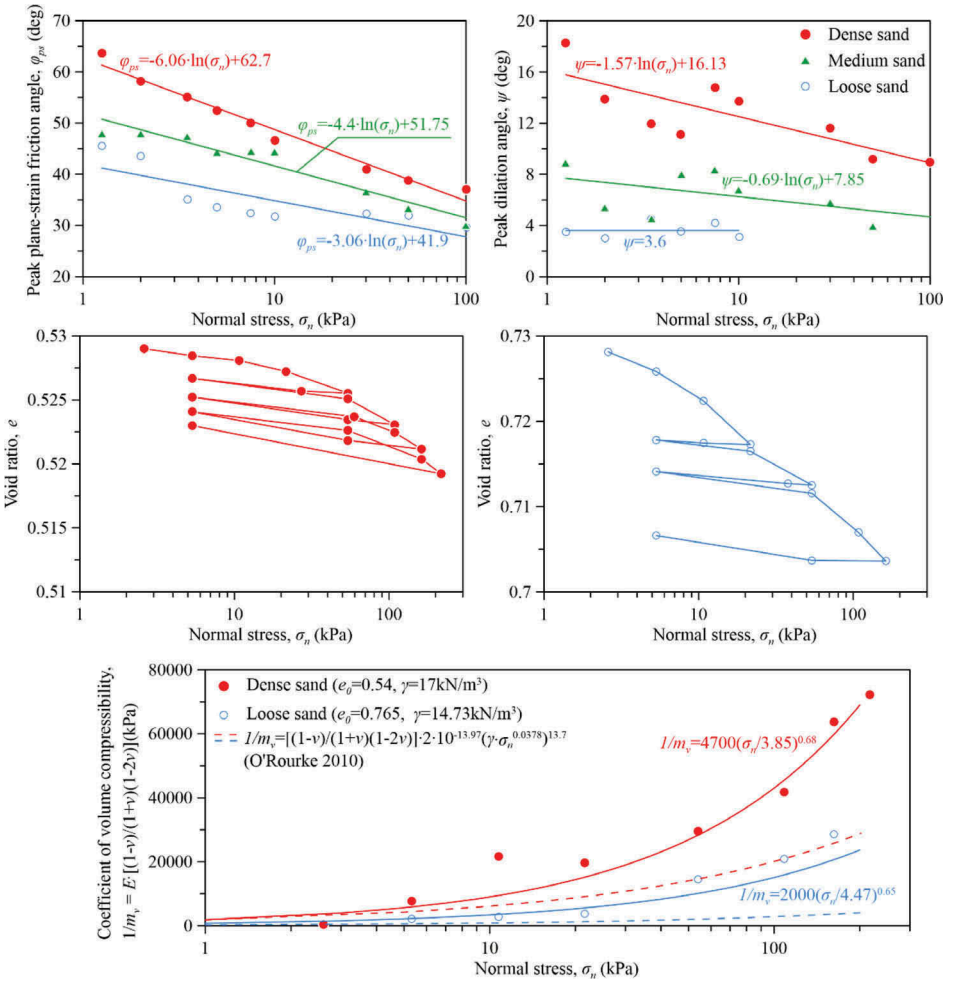

Figure 3. Variation of peak plane-strain friction angle (top left) and dilation angle (top right) of STK sand with normal stress; Variation of sand void ratio with normal stress from incremental loading oedometer tests. Results for dense sand (middle left) and loose sand (middle right); Variation of coefficient of volume compressibility interpreted from incremental loading oedometer tests for dense and loose sand (bottom). Values obtained with the fitting formula proposed by O'Rourke (2010) are also shown for comparison. E is the Young's modulus of sand and ν is the Poisson's ratio, taken for this plot ν=0.25.

compare the compressibility of loose and dense STK sand against O'Rourke's expression for partially-saturated RMS graded sand. Notice that the equivalent modulus formula predicts coefficient of volume compressibility values that are considerably lower than the measurements of dry STK sand. The implications of this are discussed in later sections.

2.3 *Friction effects on measurements*

The small width of the chamber allows testing of pipes with length-over-diameter ratio between 2 and 0.5. Therefore, the measured reaction force-pipe displacement curves must be corrected for friction between the glass walls of the chamber and the pipe, as well as the sand bed. The former component of friction is relatively straightforward to quantify, using the technique described in Ansari et al. (2018a). More specifically, every experiment is repeated after the chamber is emptied from sand, with the pipe forced to follow the same trajectory-the

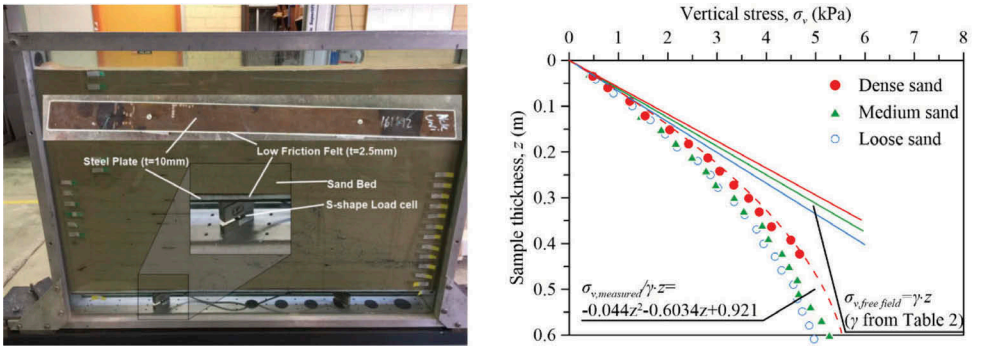

Figure 4. Setup used to measure vertical sand stress during deposition (left) and comparison of measured values against the theoretical (free field) geostatic stress distribution for different sand densities (right). The parabolic function used to correct results of tests in dense sand is also shown.

measured reaction during this "friction" test corresponds to glass-pipe friction. Such friction tests allow accounting also for the friction developing at the contact of pulleys and cable, and correcting results for it.

Friction between the glass walls and sand alters the geostatic stress field inside the chamber due to arching effects, and also increases the resistance developing on the failure wedge. In order to be able to correct measurements for sand-glass friction, the following are required: i) the distribution of geostatic vertical stresses inside the chamber; ii) the friction stress at the sand-glass interface; iii) the shape of the failure wedge. The distribution of vertical stresses was measured experimentally during deposition, using the setup shown in Figure 4. Two sets of load cells allow measuring simultaneously and continuously the total stress applied at the bottom of the chamber, and the total weight of the deposited sand. From those measurements we obtain the distribution of stresses shown in Figure 4 for loose, medium and dense sand beds. Accordingly, we can use an equivalent, reduced unit weight $\gamma_{eff}=\sigma_{v,measured}/z$ to fit the measurements of vertical stresses, and account for arching effects. This approximation is reasonably accurate for relatively shallow depths, which are of interest here.

In order to quantify friction between sand and the glass windows, we employed numerical back-analyses of the deposition process, underpinned by measurements of sand settlement during deposition using the PIV technique. In addition, we performed direct shear tests to measure directly friction at the sand-glass interface, for low normal stresses pertinent to the experimental setup. For that we used a custom direct shear apparatus with box dimensions 100mm x 100mm x 42mm, equipped with sensitive 0.5kN load cells and LVDT's. Results of these tests are depicted in Figure 5. The peak interface friction coefficient $\mu=\tau_{max}/\sigma_n$ is about $\mu=0.32$ for dense sand and $\mu=0.30$ for loose sand hence the interface friction angle that was used to correct the results that

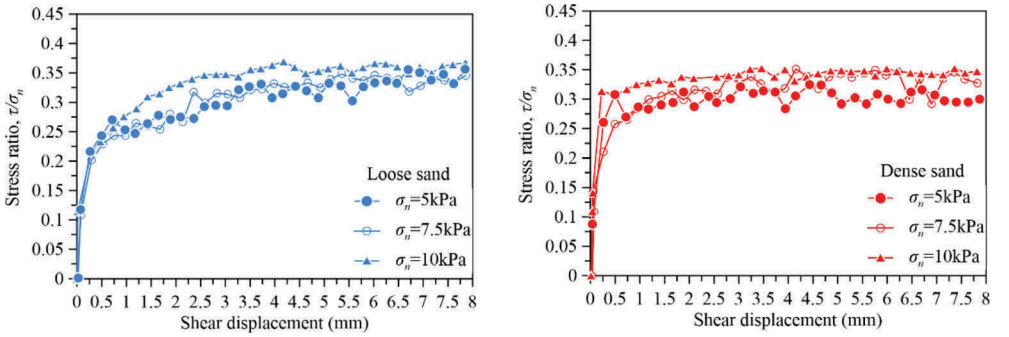

Figure 5. Measurements of friction resistance at the sand-glass interface via direct shear tests on loose (left) and dense (right) sand samples.

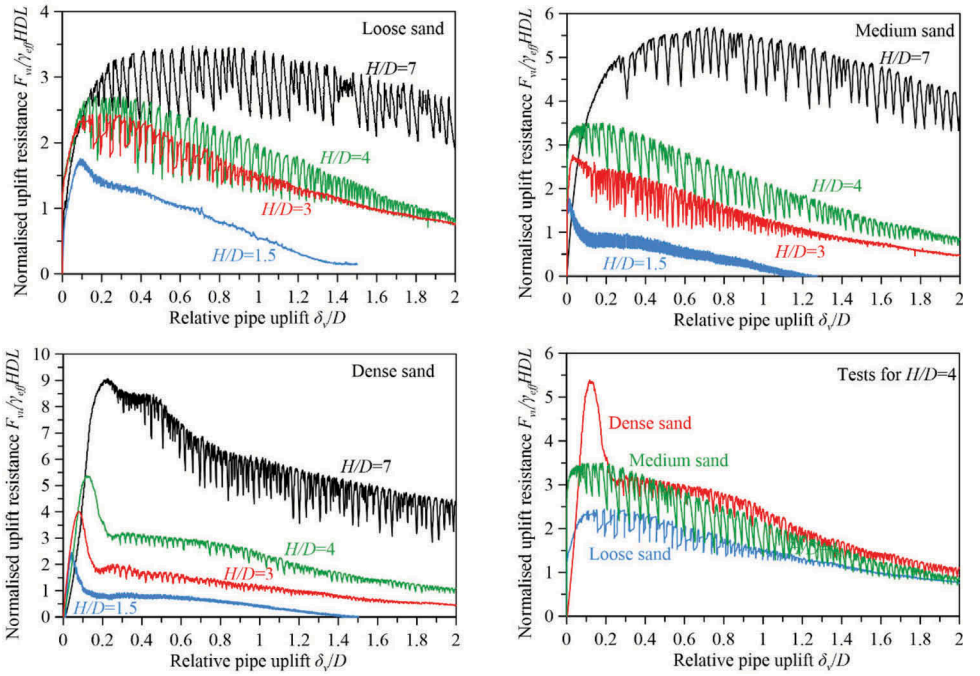

Figure 6. Plots of normalised reaction developing on the pipe during uplift tests, as function of vertical pipe displacement.

follow was $\delta=\tan^{-1}(0.32)=18°$ for tests in dense sand and $\delta=17°$ for tests in loose sand. These values are slightly higher than the values reported in Ansari et al. (2018a). Accordingly, friction between the failure wedge and glass walls is estimated from the geometry of the mobilised sand mass obtained from PIV analysis and the horizontal stress inside the chamber, assuming at-rest earth pressures along the plane perpendicular to the glass walls. Finally, we must mention that friction between the cable and sand was measured by pulling a free cable embedded in sand, and was found to be negligible compared to the other components of reaction.

2.4 *Experimental results*

To limit the length of the presentation, in the following we discuss selected results from pull-out tests only, which can be used to determine the parameters of vertical-upwards springs in a Winkler model of a pipe crossing a normal or reverse fault. First, we present in Figure 6 the normalised reaction developing on the pipe during vertical pull-out tests, as function of the normalised vertical pipe displacement. The measured reaction F_{vu} is corrected for friction effects according to the mentioned in section 2.3, and is normalised here against the weight of the soil column above the pipe $\gamma_{eff}HDL$; where γ_{eff} is the effective unit weight of sand corrected for arching effects; D is the diameter of the pipe; L is its length; H is the embedment depth measured from the pipe centreline. In addition, the vertical upwards displacement of the pipe δ_v is normalised against the pipe diameter, which in the tests at hand is D=75mm.

Figure 6 illustrates results from tests in loose, medium and dense sand, performed for a range of initial pipe embedments H/D=1.5 to 7. As expected, the peak reaction force on the pipe increases with sand density and embedment depth, and the response changes from softening to hardening as the embedment depth decreases and the density of sand increases. It is worth clarifying that the oscillations observed in the reaction post-peak are not instrument noise, but rather characteristic of stick-slip response: tests were performed while pulling the pipe at a constant rate (180mm/hr), therefore each drop in the reaction corresponds to the point where static friction resistance is exceed by the tension in the cable, and the pipe starts moving. Then, tension

is released as the coefficient of friction drops to its kinetic value, the pipe slows down again, and the process is repeated. Notice also that, irrespective of sand density, the reaction measured during tests starting from the same embedment converges to the same residual value. At large pipe displacement the response is governed by the critical state sand response, and eventually all tests converge to zero reaction, as the pipe is pulled out of the sand bed.

In order to delve a bit further into the response observed at large pipe displacements, we plot in Figure 7 the normalised reaction on the pipe in terms of its position during each test, relatively to the surface of the sand bed. We focus on 4 tests performed in dense sand, and shallow initial pipe embedment depths H/D=1.5 to 3.75. Observe that the response at large pipe displacements appears to be independent of its initial embedment, and a function of the current pipe position only: every test ends up on a steady-state line, and the reaction on the pipe decreases to a residual value as its vertical displacement increases, and sand overburden decreases. The peak reaction is governed by a progressive failure mechanism, and the formation of a wedge which geometry is a function of the dilatancy angle of sand (Figure 7). The angle θ defining the inclination of the legs of the trapezoidal wedge was determined from PIV analysis to be approximately equal to the dilation angle of sand, and increases as we approach the surface, where dilatancy increases due to the reduced confining stress (Figure 3). This suggests that, at least for the embedment depths considered here, we can describe the peak reaction developing on pipes in dense sand with a simple limit-equilibrium analytical model, such as the ones proposed by White et al. (2001) or Ansari et al. (2018a). Such a model will be able to capture the increase in the dimensionless reaction force as the embedment depth increases, given that the dimensions of the failure wedge are function of the embedment depth. Note here that assuming that the angle formed by the legs of the wedge and the vertical is equal to the peak friction angle of sand (O'Rourke & Liu 2012) will result in grossly overestimating the dimensions of the failure prism.

Next we will investigate how sensitive these results are to the diameter of the test pipe. The goal of this investigation is two-fold: First, to confirm that the proposed shallow failure mode is not sensitive to the pipe diameter, at least for the test conditions at hand. Second, to show that for the range of pipe diameters considered, normalisation of the reaction force against the weight of the sand column above the pipe (or the reaction stress against the geostatic stress at the pipe springline) results in dimensionless reaction-displacement curves. For that we performed a series of additional tests on pipes with diameters 37.5mm and 150mm i.e. half and twice the diameter of our benchmark test pipe, respectively. These tests were performed on pipes initially embedded at depths H/D=1.5 to 3.75 in dense sand, as the tests shown in Figure 7. Results are summarised in Figure 8, and are very similar for all three pipes, regardless if we examine the incremental deviatoric strains at peak reaction, normalised reaction-displacement curves or the variation of the normalised peak reaction $N_{qv}=F_{vu,peak}/\gamma_{eff}HDL$ with the initial pipe embedment H/D. Of course, results cannot be simply generalised to (very) large diameter pipes, as the shear strength of sand depends on the mean stress level. To account for that, Ansari et al. (2018a) proposed to normalise the peak vertical reaction stress acting on the pipe $F_{vu,peak}/DL$ against the peak shear strength of sand at the pipe spring line $\gamma_{eff}H\tan\varphi_{ps}$

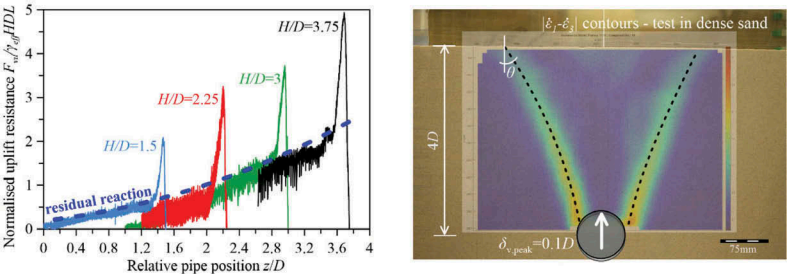

Figure 7. Plots of normalised reaction developing on the pipe during uplift tests in dense sand, as function of pipe position (left) and incremental deviatoric strain contours at peak reaction, obtained via PIV analysis of a test performed in dense sand, from initial pipe embedment H/D=4 (right).

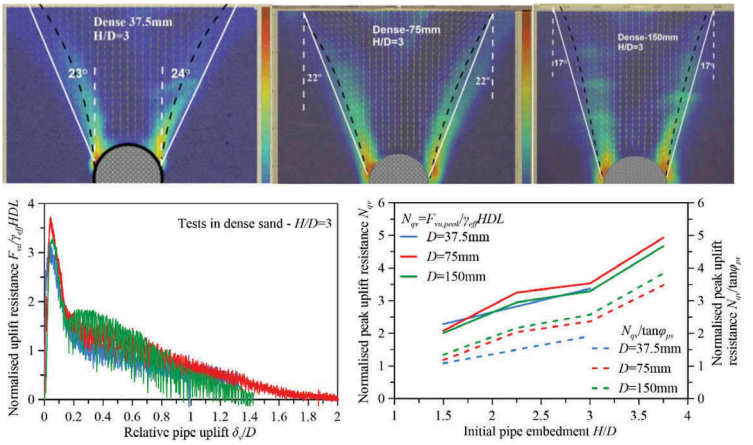

Figure 8. Diameter effects on measurements: Incremental shear strain contours and displacement vectors at peak reaction during testing of a pipe embedded in dense sand at H/D=3 (top); Plots of normalised reaction developing on the pipe, as function of its vertical displacement (bottom left); Peak reaction force measured during tests in dense sand using pipes of different diameters, as function of the initial pipe embedment (bottom right).

(instead of the geostatic stress $\gamma_{eff}H$). The variation of the normalised peak reaction $F_{vu,peak}/\gamma_{eff}HDL\tan\varphi_{ps}$ with initial pipe embedment also shown in Figure 8 suggests that for the range of pipe diameters considered, both dimensionless parameters can be used to normalise results with respect to the pipe diameter.

Given the excellent agreement of results obtained with the D=37.5mm pipe with the larger diameter pipes, we will next attempt to define the range of validity of the wedge-type failure mechanism (Figure 7). ALA (2005) and PRCI (2009) guidelines mention that the expressions provided to calculate the properties of vertical uplift soil springs are valid for embedment depths H/D<10, while Yimsiri et al. (2004) calculated numerically the "critical embedment ratio H_c/D", where the peak dimensionless reaction force does not further increase with an increase in embedment depth, to be H_c/D=30 for dense sand. Yimsiri et al. (2004) also reported that the peak dimensionless force at the critical embedment is $F_{vu}/\gamma_{eff}HDL$=25 for dense sand. In order to determine experimentally the critical embedment ratio of pipes in dense sand, we performed a series of uplift tests with the D=37.5mm pipe initially embedded at depths H/D=1.5 to 18. Results of these tests are summarised in Figure 9, in the form of plots of the normalised reaction on the pipe as function of the position of the pipe during each test.

Notice that there is a clear shift from softening to hardening response as the embedment depth of the pipe increases. Indeed, a critical embedment ratio H_c/D is identified in Figure 9 and the peak dimensionless reaction force does not increase past $F_{vu}/\gamma_{eff}HDL$=25 which, interestingly, agrees well with the findings of Yimsiri et al. Nevertheless, the critical embedment ratio found experimentally is about H_c/D=15; considerably shallower than the critical embedment ratio reported by Yimsiri et al. In addition, it is clear that the softening response observed in shallow tests is supressed at embedments deeper that H/D=10. This suggests that the wedge-type model is not appropriate for describing the reaction developing on deeply buried pipes, but also that the transition to a constant normalised reaction force at the critical embedment is not only due to reduced dilatancy potential of sand, but also due to a change in the failure mode. Evidence on that is drawn if we examine contours of incremental deviatoric strains and displacement vectors at peak reaction force from a test starting at H/D=3 and a test starting at H/D=18 (Figure 10). It is clear that at large embedment depths a flow-around deep mechanism develops, resulting in constant normalised force as the dimensions of the failure surface are independent of the embedment of the pipe; unlike the case of the shallow failure mechanism, where the dimensionless reaction force increases as the pipe embedment and the size of the failure wedge increase. Notice also in Figure 9 that the pipe displacement

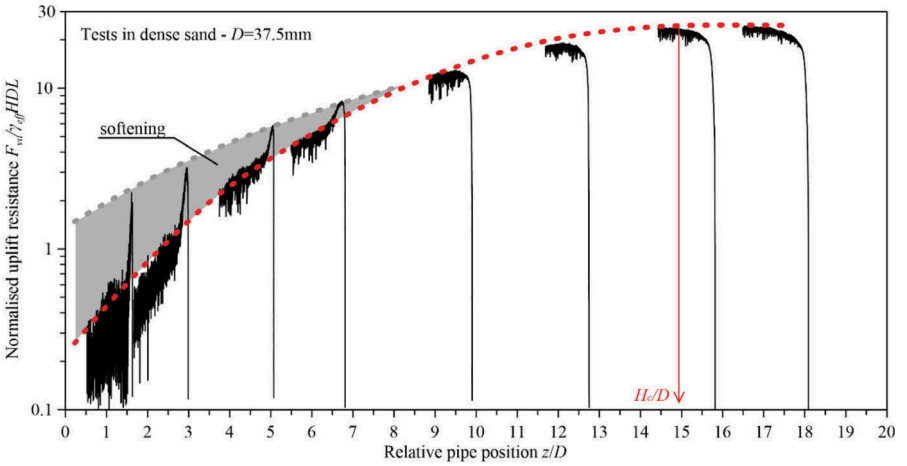

Figure 9. Determination of the critical embedment ratio H_c/D from uplift tests in dense sand, by plotting the normalised reaction developing on the pipe as function of pipe position during the tests.

required to reach the peak reaction increases considerably as the pipe embedment increases; for tests performed with the pipe embedded at $H/D>15$ the reaction keeps increasing until we reach pipe displacements of the order of $0.8D$-$1.0D$.

Findings from tests in dense sand at pipe embedment up to and beyond the critical embedment ratio are summarised in Figure 11, where we plot the variation of the normalised peak uplift reaction with initial pipe embedment. Figure 11 also presents the experimental results of Trautmann et al. (1985) obtained from uplift tests on 102mm pipes embedded in dense Cornell filter sand, and the numerical results of Yimsiri et al. (2004), which were calibrated on Trautmann et al.'s experiments. Notice that good agreement is observed for shallow embedment depths, especially if we use Ansari et al.'s dimensionless reaction force to compare results. Nevertheless, as mentioned above, experimental results suggest that a deep failure mode governs the response

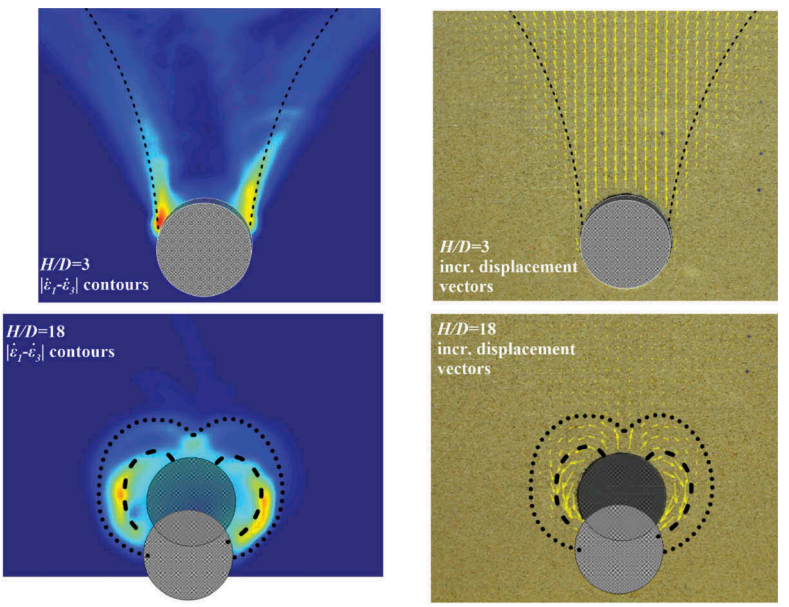

Figure 10. Incremental shear strains and displacement vectors at peak reaction force obtained from PIV analysis of tests in dense sand, with the pipe initially embedded at $H/D=3$ (top) and $H/D=18$ (bottom).

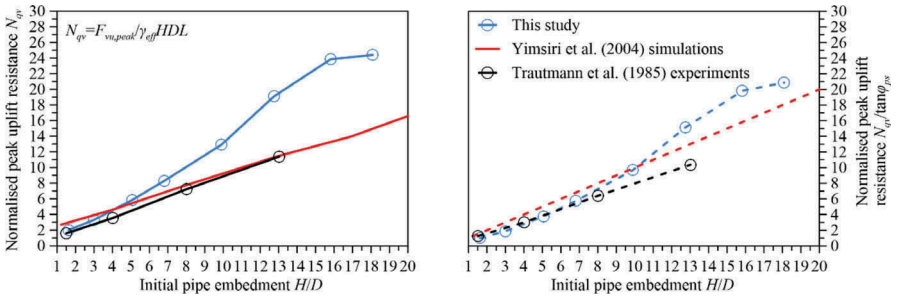

Figure 11. Peak reaction stress F_{vu}/DL on the pipe normalised against the geostatic stress at the pipe springline $(F_{vu}/DL)/\gamma_{eff}H$ (left) and against the peak shear strength of sand at the pipe springline $(F_{vu}/DL)/\gamma_{eff}H\tan\varphi_{ps}$ (right), plotted against the initial embedment ratio.

of pipes embedded deeper than H/D=15, and higher reaction forces were measured for embedment depths H/D>13 compared to published studies. Analysis of tests results performed in loose and medium sand is ongoing, as well as of oblique uplift tests, where the direction of pipe movement forms an angle with the vertical, as it will be the case in oblique fault crossings.

3 NUMERICAL MODELLING OF TRENCH-BACKFILL-PIPE INTERACTION

3.1 *General*

One of the limitations of the experiments presented thus far is that they apply to uniform backfill conditions, comprising dry sand. In practice, although buried pipes are backfilled with coarse-grained material, they are laid in (narrow) trenches excavated in the natural soil. If the natural soil is considerably stiffer/stronger than the backfill, the reaction force applied on the pipe during a differential movement episode will be higher, resulting in higher pipe strains. As a result, design guidelines recommend "*Soil properties representative of the backfill should be used to compute axial soil spring forces. Other spring forces should generally be based on the native soil properties"* (ALA 2005). This provision will unavoidably lead to (costly) mitigation measures when trenches are formed in stiff soil/rock formations, as the beneficial contribution of the loose backfill to reducing stresses on pipe is ignored. Nevertheless, the ALA recommendations continue *"Backfill soil properties are appropriate for computing horizontal and upward vertical spring forces only when it can be demonstrated that the extent of pipeline movement relative to the surrounding backfill soil is not influenced by the soils outside the pipe trench"*. In other words, we can design the dimensions of the trench to limit interaction of the pipe with its backfill soil only. If this is not applicable in practice, e.g. due to the very large dimensions of the required excavation, we should quantify the contribution of the native soil to the reaction developing on the pipe, for given trench dimensions.

Owing to the multiple parameters affecting the problem of trench-backfill-interaction, physical modelling experiments cannot but cover only very limited cases. Instead, the approach followed in the recent literature on this topic (Kouretzis et al. 2013, Chaloulos et al. 2015, 2017, Limnaiou et al. 2018, 2019, Kouretzis et al. 2014) is to perform parametric numerical analyses considering different relative movement directions and backfill properties, but mainly different trench geometry configurations. One of the main challenges when it comes to simulating the problem at hand is the fact that complex failure mechanisms involving large displacements govern the reaction developing on the pipe, even if we are not interested in capturing the softening part of the response, following ALA (2005) assumption that the *"spring force is constant once it reaches its maximum value"*. Indeed, we have shown in Figure 6 that even for embedment ratios up to H/D=4, that are of interest for buried oil and gas pipes in shallow trenches, the pipe displacement required to reach the peak reaction may be of the order of 20-30% of the pipe diameter. To address that, the numerical methods employed to simulate this complex problem are based on techniques that alleviate the effects of mesh distortion, such as Arbitrary

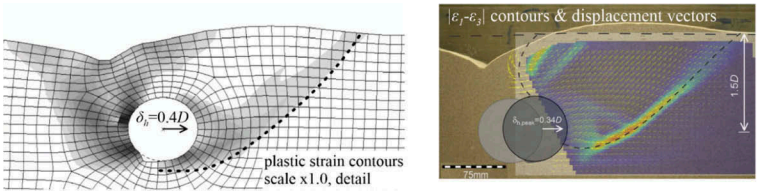

Figure 13. Comparison of failure prism obtained from large displacement finite element analysis (left, Kouretzis et al. 2013) and from PIV analysis of lateral drag tests (right, Ansari et al. 2019). Results from simulations/tests in loose sand and pipe embedment H/D=1.5

Lagrangian-Eulerian (ALE) remeshing (Kouretzis et al. 2013), mesh rezoning (Chaloulos et al. 2015, 2017, Limnaiou et al. 2018, 2019) or adaptive remeshing (Kouretzis et al. 2014, Ansari et al. 2018b). The numerical models used in the abovementioned studies were calibrated on independent experimental results (Trautmann & O'Rourke 1985, Trautmann et al. 1985) and, as discussed in Ansari et al. (2018b) which presents a series of "blind" numerical predictions of uplift tests, advanced numerical methods are capable of capturing the essential mechanics of the problem, at least in cases where shallow mechanisms prevail (see Figures 13 & 14). Selected outcomes of these studies i.e. the trench dimensions required to confine failure inside the backfill, or the increase in the reaction developing on the pipe for cases where excavating a very large trench is uneconomical, are summarised in the following.

3.2 *Effect of trench dimensions on reaction developing on pipes in strike-slip fault crossings*

The first approach to alleviating the influence of the (stiff) natural ground on the reaction developing on the pipe is to design the geometry of the trench so that the failure surface (Figure 13) develops entirely within the backfill soil. Kouretzis et al. (2013) determined the dimensions of the failure surface from numerical simulations of lateral pipe movements, and proposed to lay pipes in a trapezoidal trench with dimensions determined according to Figure 15. The mentioned numerical study is limited to cases of pipes embedded in relatively shallow trenches backfilled with loose-to-medium sand, which is required to minimize the reaction on the pipe. Kouretzis et al. (2014) propose a similar nomograph for pipes subjected to vertical-downwards relative movements, however they note that the size of the trench to ensure that the reaction force is not influenced by the stiff natural soil and thus to satisfy ALA (2005) recommendations may be excessive. Therefore, they recommend to perform project-specific analyses to quantify the increase in pipe reaction due to interaction with the natural ground, and optimize the design.

The latter approach was followed by Chaloulos et al. (2015, 2017), who quantified the increase in the reaction developing on the pipe during lateral movements as function of the dimensions of the trench. They assumed that the natural ground where the trench is excavated is very stiff compared to the backfill, hence can be modelled as rigid, and investigated both rectangular and trapezoidal trench shapes. Selected results of their study for a shallowly

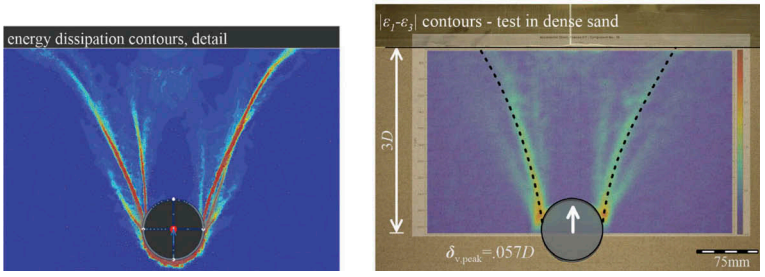

Figure 14. Comparison of failure prism obtained from finite element analysis with adaptive meshing (left, Ansari et al. 2018b) and from PIV analysis of uplift tests (right, Ansari et al. 2018a). Results from simulations/tests in dense sand and pipe embedment H/D=3.

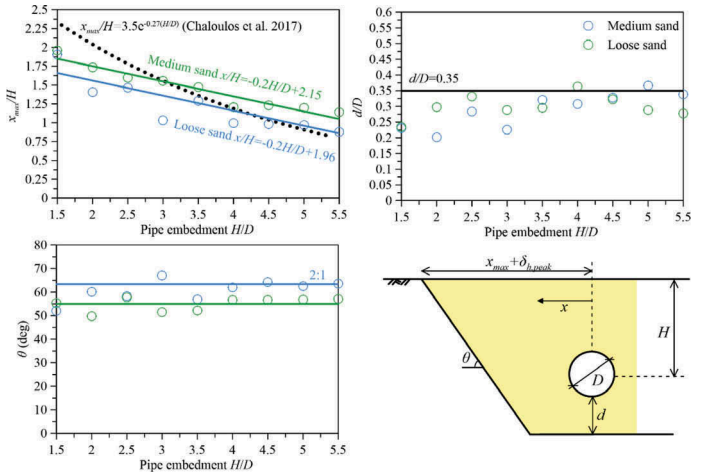

Figure 15. Determination of minimum trench dimensions to eliminate interaction with the surrounding natural ground (after Kouretzis et al. 2013). $\delta_{h,peak}$ is the maximum anticipated horizontal pipe displacement.

buried pipe (H/D=1.5) are summarized in Figure 16, which depicts the increase in the normalised reaction force as function of the width of the trench x, and the depth of the trench measured from the pipe invert d (Figure 15). Note that Chaloulos et al. (2017) normalize the width of the trench x against the width of the failure surface x_{max}, which they proposed to calculate from the following approximate expression, resulting from the interpretation of a series of parametric numerical analyses:

$$x_{max}/H=3.5e^{-0.27(H/D)} \tag{2}$$

As depicted in Figure 15, this expression agrees well with the results of Kouretzis et al. (2013) and provides a safe upper bound of the size of the failure wedge for shallowly buried pipes. Notice also in Figure 16 that the reaction applied on the pipe increases exponentially as the trench becomes narrower. For example, a pipe buried in H=1.5D will experience twice the

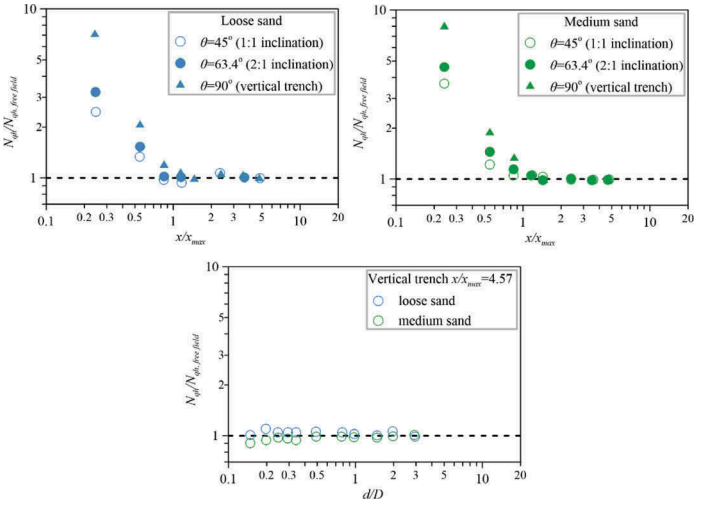

Figure 16. Effect of trench width, sand density and trench inclination (top) and of vertical trench depth (bottom) on ultimate reaction from soil (after Chaloulos et al. 2017). Results for embedment depth H/D=1.5. x_{max} denotes the width of the failure surface (see Eq. 2).

reaction if, instead of uniform sand, it is embedded in a vertical trench with half-width about x=1.75D (plus the fault displacement applied on the pipe $\delta_{h,peak}$). A two-fold increase in pipe lateral reaction will result in an increase in pipe bending strains of the order of 100%; that's for a pipe buried in a trench wider than 3.5D in total, much wider than standard construction practice. Laying the pipe into a trapezoidal trench will lessen the effect of the stiff ground on reactions (Figure 16), at the expense of increased excavation costs. On the other hand, the depth of the trench has a trivial effect on the reaction developing on the pipe during lateral relative movements. Similar results for the effect of trench dimensions on the ultimate uplift and vertical-downwards reaction on pipes laid in trenches excavated in rock are presented by Limnaiou et al. (2018) and Limnaiou et al. (2019), respectively.

We must mention here though that modelling sand as elastoplastic material obeying the Mohr-Coulomb failure criterion (an assumption adopted in the abovementioned numerical studies) requires using an equivalent Young modulus for sand to replicate experimental reaction-displacement curves. This equivalent modulus is not representative of sand stiffness (see Figure 3), as it incorporates the effects of slack in the loading system, an issue identified by Trautmann et al. (1985) and Ansari et al. (2018a). This implies that the displacement required to reach the peak reaction on the pipe measured experimentally and replicated numerically with models calibrated on reaction-displacement measurements is an upper bound of the actual pipe displacement at peak reaction, and should be treated as such when determining properties of Winkler springs in practice. In addition, using equivalent sand properties does not allow capturing the response of pipes in loose-to-dense backfills without altering the model calibration, thus each of the studies of Kouretzis et al. (2013), Chaloulos et al. (2015, 2017) and Yimsiri et al. (2004) is limited to a rather narrow range of sand densities.

Finally, we must stress out that as the embedment of the pipe increases and the failure mechanism changes from a passive wedge-type to a flow-around mechanism, the accuracy of continuum-based numerical analysis methods decreases, as the pipe displacement required to reach the peak reaction is of the order of one pipe diameter. Ansari et al. (2018b) used a variation of the Hardening Mohr-Coulomb model (Doherty and Muir Wood 2013) to shown that "blind" numerical predictions of the peak reaction developing on pipes are possible without using equivalent constitutive model parameters, but only for relatively shallow pipes. These findings are applicable not only to plane-strain models of rigid pipes subjected to relative displacements but are also relevant to more complex three-dimensional models of the pipe and its surrounding backfill/soil.

4 CONCLUDING REMARKS

The high-quality experimental measurements summarised in this paper, augmented with PIV and close-range photogrammetry analysis of sand displacements during pipe movement, shed some light on the mechanisms of sand-pipe interaction, and allowed us to identify some limitations in current practice. We presented evidence that the mechanism leading to the development of reaction on the pipe during uplift relative displacement episodes depends on the density of the backfill, but also on the embedment depth of the pipe. We have shown that the assumption of a wedge-type failure mode, on which analytical models used to estimate the peak reaction on the pipe are based on, is realistic for pipes embedded in dense sand, at shallow depths H/D<5. For such depths, the formation of a symmetric trapezoid failure prism when the peak reaction is reached was confirmed via PIV analyses, with the inclination of the legs of the prism not being constant, but a function of the dilation angle of sand. At larger pipe displacements, the reaction on the pipe drops to a residual value, which is a function only of this current overburden and not of its initial embedment. As the initial pipe embedment increases beyond H/D=5 the response changes from softening to hardening, and at depths larger than about H/D=15 a local, flow-around failure mode is observed. Beyond this "critical" pipe embedment the normalised (against the geostatic stress) reaction stress applied on the pipe no longer increases with pipe embedment, as the size of the failure surface remains constant. Therefore, current limit-equilibrium models proposed to determine the peak

reaction on the pipe cannot capture the mechanics of the problem for deeply embedded pipes. We also observed that, at least for dense sand, this transition to a flow-around failure mode takes place at depths considerably shallower compared to published numerical results, which may lead to un-conservative estimates of the reaction on pipes embedded at depths $13<H/D<30$ e.g. pipes underneath embankments.

In the second part we briefly show that advanced numerical methods for modelling relative soil-rigid pipe movements are capable of capturing the shape of the failure mechanism observed in PIV analysis, at least for shallow embedment depths. Modelling this problem requires the use of techniques to alleviate mesh distortion, as pipe displacements required to reach the peak reaction force are relatively large, even for shallowly buried pipes in dense sand. Finally, we discussed the application of numerical methods for quantifying the effect of the dimensions of the trench in which pipes are usually laid, on the reaction developing on pipes affected by strike-slip fault rupture. If the trench is excavated in very stiff (compared to the backfill material) natural ground, and its lateral extent is not sufficient to encapsulate the failure surface, the reaction on the pipe may be one order of magnitude higher than the reaction developing in uniform backfill conditions, for which methods for calculating Winkler spring properties apply to. Excavating trenches wide enough to ensure that interaction between the pipe and its surrounding backfill is not affected by the stiff natural soil is not always economical. In practice, the dimensions of the trench in crossings with active faults should result from an optimization procedure, considering excavation and backfill material costs, design fault movements and the cost of strengthening the pipe itself.

ACKNOWLEDGMENTS

Part of the work presented in this paper is supported by the Australian Research Council (Projects DP150102508 & DP180103497). The authors also wish to acknowledge the contributions of Dr. Yousef Ansari, Dr. Yiannis Chaloulos, Dr. Jubert Pineda, Dr. Laxmi Suwal and Mr. Jinbiao Wu.

REFERENCES

ALA 2005. *Guidelines for the design of buried steel pipes*. American Lifelines Alliance (ALA), ASCE,

Ansari, Y., Kouretzis, G. & Sloan, S.W. 2018a. Development of a prototype for modelling soil-pipe interaction and its application for predicting the uplift resistance to buried pipe movements in sand. *Canadian Geotechnical Journal* 55:1451–1474.

Ansari, Y., Kouretzis, G. & Pineda, J. 2018b. Sand-pipe interaction at fault crossings: Experimental and numerical investigation. In *Proceedings of the 16th European Conference on Earthquake Engineering*.

Ansari, Y., Kouretzis, G. & Sloan, S.W. 2019. Physical modelling of lateral sand-pipe interaction. *Géotechnique* (under revision)

Chaloulos, Y. K., Bouckovalas, G. D. & Karamitros, D. K. 2017. Trench effects on lateral p-y relations for pipelines embedded in stiff soils and rocks. *Computers and Geotechnics* 83:52–63.

Chaloulos, Y. K., Bouckovalas, G. D., Zervos, S. D. & Zampas, A. L. 2015. Lateral soil–pipeline interaction in sand backfill: effect of trench dimensions. *Computers and Geotechnics* 69:442–451.

Cheuk, C.Y., White, D.J. & Bolton, M.D. 2008. Uplift mechanisms of pipes buried in sand. *Journal of Geotechnical and Geoenvironmental Engineering* 134(2):154–163.

Davis, E.H. 1968. Theories of plasticity and the failure of soil masses. Chapter 6. In Lee, K. (ed.), *Soil Mechanics Selected Topics*.

Doherty, J.P. & Muir Wood D. 2013. An extended Mohr-Coulomb (EMC) model for predicting the settlement of shallow foundations on sand. *Géotechnique* 63:661–673.

Dickin, E.A. 1988. Uplift behavior of horizontal anchor plates in sand. *Journal of Geotechnical Engineering* 114(11):1300–1317.

EERI 1999. *The Izmit (Kocaeli), Turkey Earthquake of August 17, 1999*. EERI Special Earthquake Report.

Hall, W.J., Nyman, D.J., Johnson, E.R. & Norton, J.D. 2003. Performance of the Trans-Alaska pipeline in the November 3, 2002 Denali fault earthquake. In *Advancing Mitigation Technologies and Disaster Response for Lifeline Systems* 522–534.

Jung, J.K., O'Rourke, T.D. & Argyrou, C. (2016). Multi-directional force–displacement response of underground pipe in sand. *Canadian Geotechnical Journal* 53(11):1763–1781.
Karamitros, D.K., Bouckovalas, G.D. & Kouretzis, G.P. 2007. Stress analysis of buried steel pipelines at strike-slip fault crossings. *Soil Dynamics and Earthquake Engineering* 27(3):200–211.
Karamitros, D., Bouckovalas, G., Kouretzis, G. & Gkesouli, V. 2011. An analytical method for the strength verification of buried steel pipelines at normal fault crossings. *Soil Dynamics and Earthquake Engineering* 31(11):1452–1464.
Kouretzis, G., Sheng, D. & Sloan, S.W. 2013. Sand-pipeline-trench lateral interaction effects for shallow buried pipelines. *Computers and Geotechnics* 54:53–59.
Kouretzis, G., Krabbenhoft, K., Sheng, D. & Sloan, S.W. 2014. Soil-buried pipeline interaction for vertical downwards relative offset. *Canadian Geotechnical Journal* 51(10):1087–1094.
Kouretzis, G., Karamitros, D. & Sloan, S.W. 2015. Analysis of buried pipelines subjected to ground surface settlement and heave. *Canadian Geotechnical Journal* 52:1058–1107.
Limnaiou, T.G., Housos, A.G., Chaloulos, Y.K. & Bouckovalas, G.D. 2018. Uplift resistance of pipelines embedded in stiff soils and rocks: Effect of trench dimensions. In *Proceedings of the 16th European Conference on Earthquake Engineering*.
Limnaiou, T., Tsifis, C., Bouckovalas G. & Chaloulos, Y. 2019. Effect of trench dimensions on the vertical resistance of pipelines embedded in stiff soils and rocks. In *Proceedings of the 7th International Conference on Geotechnical Earthquake Engineering*.
Lings, M.L. & Dietz, M.S. 2004. An improved direct shear apparatus for sand. *Géotechnique* 54:245–256.
Majer, J. 1955. Zur berechnung von zugfundamenten. *Osterreichische Bauzeitschrift 10*(5):85–90.
NEN3650 1992. *Requirements for steel pipeline transportation systems*. Nederlands Normalisatie Instituut.
Newmark, N.M. & Hall, W.J. 1975. Pipeline design to resist large fault displacement. In *Proceedings of US National Conference on Earthquake Engineering* 416–425.
O'Rourke, T.D. 2010. Geohazards and large, geographically distributed systems. *Géotechnique* 60:505–543.
O'Rourke, M.J. & Liu, X. *Seismic design of buried and offshore pipelines*. MCEER-12-MN04
Palmer, M.C., O'Rourke, T.D., Stewart, H.E., O'Rourke, M.J., Symans, M. & Abdoun, T. 2006. Large displacement soil-structure interaction test facility for lifelines. In *8th US National Conference on Earthquake Engineering 2006* 5766-5774.
PRCI 2009. G*uidelines for constructing natural gas and liquid hydrocarbon pipelines in areas subject to landslide and subsidence hazards*. RPCI Pipeline Research Council International Inc.
Stanier, S.A., Blaber, J., Take, W.A. & White, D.J. 2015. Improved image-based deformation measurement for geotechnical applications. *Canadian Geotechnical Journal* 53(5):727–739.
Trautmann, C.H. & O'Rourke, T.D. 1985. Lateral force-displacement response of buried pipe. *Journal of Geotechnical Engineering* 111(9):1077–1092.
Trautmann, C.H., O'Rourke, T.D. & Kulhawy, F.H. 1985. Uplift force-displacement response of buried pipe. *Journal of Geotechnical Engineering* 111(9):1061–1076.
Trifonov, O.V. & Cherniy, V.P. 2010. A semi-analytical approach to a nonlinear stress–strain analysis of buried steel pipelines crossing active faults. *Soil Dynamics and Earthquake Engineering* 30:1298–1308.
Uzarski, J. & Arnold, C. 2001. Chi-Chi, Taiwan, Earthquake of September 21, 1999, Reconnaissance Report. *Earthquake Spectra* 17:37–60.
Vazouras, P., Karamanos, S.A. & Dakoulas, P. 2010. Finite element analysis of buried steel pipelines under strike-slip fault displacements. *Soil Dynamics and Earthquake Engineering*, 30(11):1361–1376.
White, D.J., Cheuk, C.Y. & Bolton, M.D. 2008. The uplift resistance of pipes and plate anchors buried in sand. *Géotechnique* 58(10):771–779.
White, D.J., Take, W.A. & Bolton, M.D. 2003. Soil deformation measurement using particle image velocimetry (PIV) and photogrammetry. *Géotechnique* 53(7):619–631.
White, D.J., Barefoot, A.J. & Bolton, M.D. 2001. Centrifuge modelling of upheaval buckling in sand. *International Journal of Physical Modelling in Geotechnics* 1(2):19–28.
Yimsiri, S., Soga, K., Yoshizaki, K., Dasari, G.R. & O'Rourke, T. D. 2004. Lateral and upward soil-pipeline interactions in sand for deep embedment conditions. *Journal of Geotechnical and Geoenvironmental Engineering* 130(8):830–842.
Zhang, X., Sheng, D., Kouretzis, G., Krabbenhoft, K. & Sloan, S.W. 2015. Numerical investigation of the cylinder movement in granular matter. *Physical Review E* 91:022204.